Electronic Supplementary Material (ESI) for Journal of Materials Chemistry C.

Electronic Supplementary Information

Thickness-Tunable Growth of Ultra-Large, Continuous and High-Dielectric h-BN Thin Films

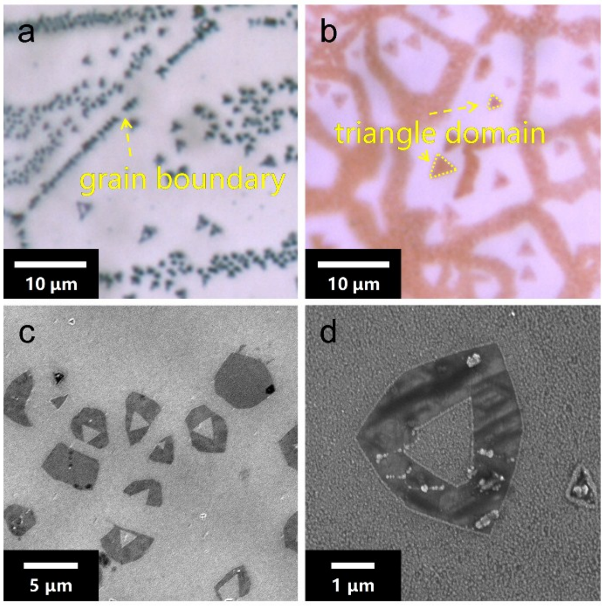

Figure S1. H_2 Etching of h-BN films during the cooling process. (a, b) Optical microscope image of h-BN films on Cu foil after etching. (c, d) SEM image of h-BN films on Cu foil after etching.

Figure S1a and S1b show the optical microscopy images of triangle-shape vacancies are etched away by H_2 during naturally cooling to room temperature at the gas flow of 45 sccm Ar/5 sccm H_2 (after the deposition process was finished). The triangle-shape vacancies are massively distributed around the grain boundaries of Cu foils, which indicate more defects of h-BN films grown upon the grain boundaries of Cu foils. Figure S1c and S1d show the SEM images of triangle-shape vacancies.

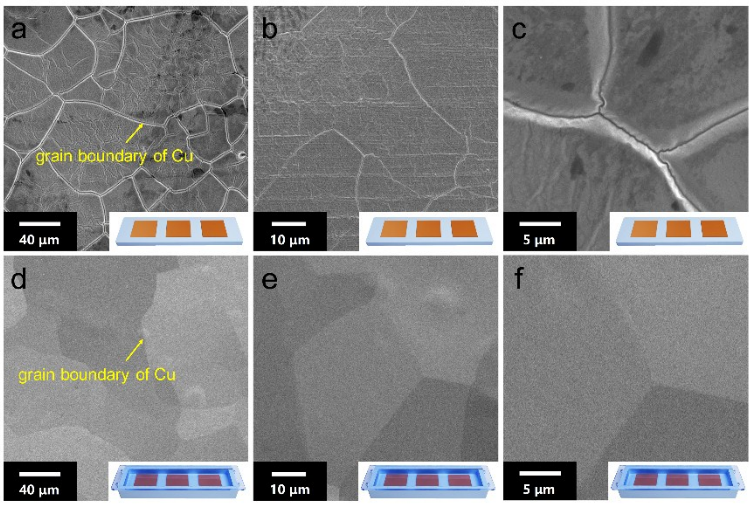

Figure S2. SEM images of h-BN films on Cu foil grown under "exposed" and "enclosure" conditions, respectively. (a-c) Morphologies of h-BN films grown under "exposed" structure. (d-f) Morphologies of h-BN films grown under "enclosure" reactor.

We compared the roughness of h-BN films between grown under "exposed" and "enclosure" conditions. Figure S2 (a-c) show the morphologies of h-BN films grown under "exposed" structure. The mismatch between different grains causes an uneven surface. The grain boundaries of Cu foil can be easily observed. Figure S2 (d-f) show the morphologies of h-BN films grown under “enclosure” reactor. The surface is smoother than Cu foil under “exposed” structure. The high partial pressure of Cu vapor in the “enclosure” reactor could help to reduce the Cu loss during annealing and obtain a smoother surface.

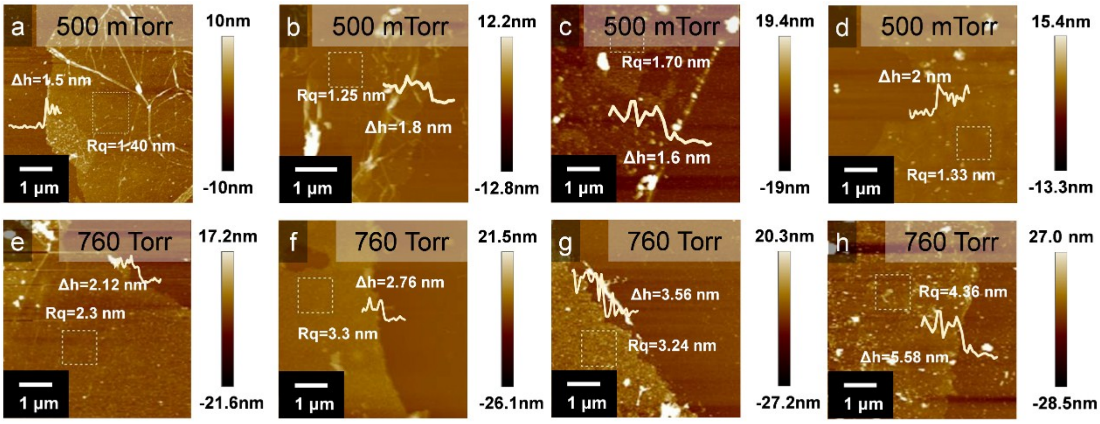

Figure S3. AFM images. (a-d) Surface morphologies of the h-BN films grown at the growth pressure of 500 mTorr and the carrier gas flow rate of 50, 100, 200, 400 sccm, respectively. (e-h) Surface morphologies of the h-BN films grown at atmospheric pressure and the carrier gas flow rate of 50, 100, 200, 400 sccm, respectively.

From the AFM images, h-BN films grown under 760 Torr show higher thickness and RMS roughness than 500 mTorr at the same carrier gas flow rate. The wrinkled surfaces of films were caused by the squeezing during h-BN deposited on the grain boundaries of Cu foil. These wrinkles could limit the carrier mobility of graphene on h-BN. So, increasing the grain size of Cu foil during annealing can be an effective way to obtain high quality h-BN films[1].

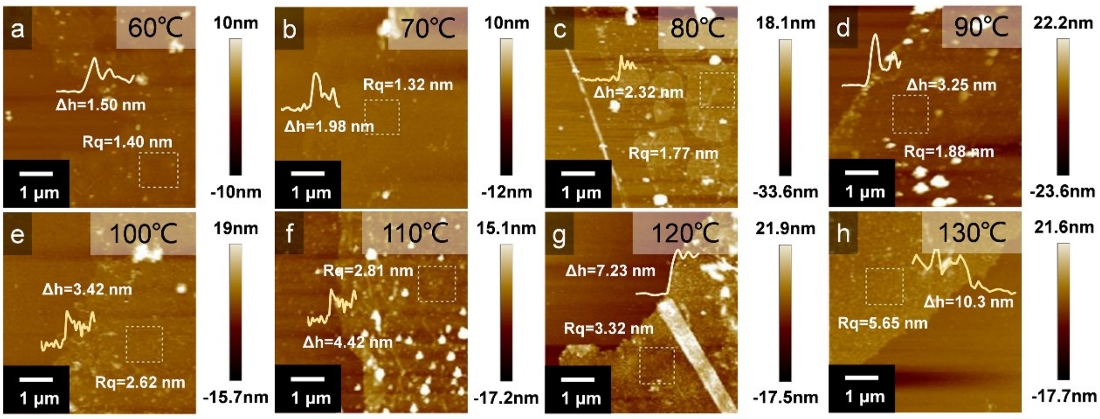

Figure S4. AFM images. (a-h) Surface morphologies of the h-BN films grown at different sublimation temperatures in a scanning area of 5 μm × 5 μm.

The thickness and RMS roughness of h-BN film increase as the sublimation temperature increases. The RMS roughness, R_q, distributes from 1.40 nm to 1.88 nm at the temperature below 90 ^{o}C, and reaches to 5.65 nm at 130 ^{o}C. Both the high growth pressure and high sublimation temperature could lead to a higher growth rate of h-BN. The growth of h-BN film could be easily converted to 3D growth at higher growth rate (Volmer-Weber growth). The high-contrast 3D clusters shown in AFM image are caused by Volmer-Weber growth[2].

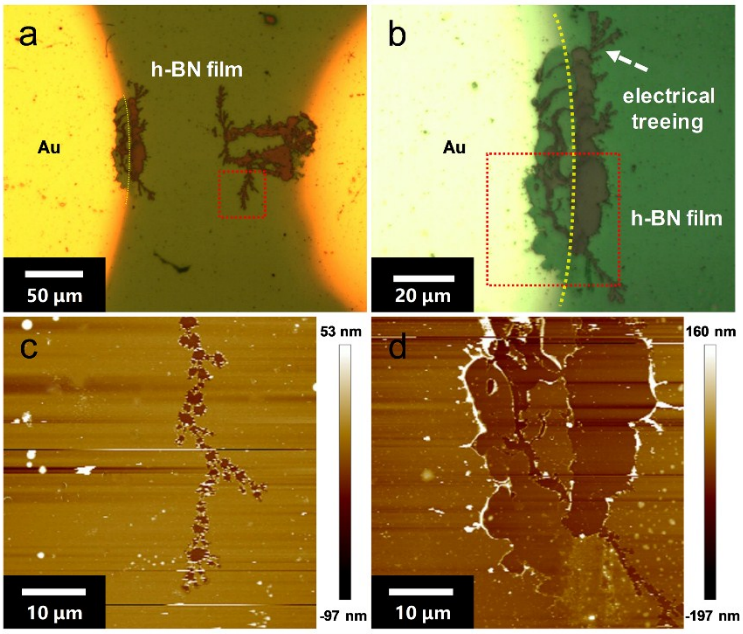

Figure S5. Optical microscopy and AFM images of h-BN film after breakdown tests.

Figure S5a and S5b show the electrode damage and catastrophic fracture of the h-BN caused by dielectric breakdown. As shown in the optical image after breakdown, the electrical tree occurs and propagates from the edge of Au electrode. The dielectric breakdown brought abruptly released energy as well as mechanical stress, which resulted in fracture propagation. Figure S5c shows the detailed image of electrical tree shown in Figure S5a. The branch-like fractured shape is similar to the former study[3]. Figure S5d shows the electrode damage caused by dielectric breakdown as shown in Figure S5b. The pattern is formed from the thermally melted Au electrode by over current.

1 S. Jin, M. Huang, Y. Kwon, L. Zhang, B. W. Li, S. Oh, J. Dong, D. Luo, M. Biswal, B. V. Cunning, P. V. Bakharev, I. Moon, W. J. Yoo, D. C. Camacho-Mojica, Y. J. Kim, S. H. Lee, B. Wang, W. K. Seong, M. Saxena, F. Ding, H. J. Shin and R. S. Ruoff, *Science*, 2018, DOI: 10.1126/science.aao3373.

2 J. C. Koepke, J. D. Wood, Y. Chen, S. W. Schmucker, X. Liu, N. N. Chang, L. Nienhaus, J. W. Do, E. A. Carrion, J. Hewaparakrama, A. Rangarajan, I. Datye, R. Mehta, R. T. Haasch, M. Gruebele, G. S. Girolami, E. Pop and J. W. Lyding, *Chemistry of Materials*, 2016, **28**, 4169-4179.

3 Y. Hattori, T. Taniguchi, K. Watanabe and K. Nagashio, *Applied Physics Letters*, 2016, **109**, 253111.